INTERSPEECH 2021
30 August – 3 September, 2021, Brno, Czechia

Comparison between Lumped-mass Modeling and Flow Simulation of the Reed-type Artificial Vocal Fold

Rafia Inaam[1], Tsukasa Yoshinaga[1], Takayuki Arai[2], Hiroshi Yokoyama[1], Akiyoshi Iida[1]

[1]Department of Mechanical Engineering, Toyohashi University of Technology, Japan
[2]Department of Information and Communication Sciences, Sophia University, Japan
rafia@aero.me.tut.ac.jp, yoshinaga@me.tut.ac.jp, arai@sophia.ac.jp,
h-yokoyama@me.tut.ac.jp, iida@me.tut.ac.jp

Abstract

The sound generated by a reed-type artificial vocal fold was predicted by a one-mass modeling and numerical flow simulation to examine the sound generation mechanisms of the artificial vocal fold. For the one-mass modeling, the reed oscillation was modeled with an equivalent spring constant, and the flow rate was estimated by Bernoulli's equation. For the flow simulation, the flow and acoustic fields were predicted with compressible Navier-Stokes Equations, while the reed oscillation was calculated by a one-dimensional beam equation. The experimentation was conducted by measuring the sound of an artificial vocal fold in an anechoic chamber. The results of the acoustic measurement showed that the sound amplitudes in the flow simulation agreed well with the experiment, while the one-mass model underestimated the amplitudes in a higher frequency range. Reed displacement and flow rate comparisons indicated that the flow retention in the reed retainer caused the asymmetry in the flow rate waveform, hence producing larger amplitudes for the flow simulation in the higher frequency range. The flow simulation enabled to predict this flow retention which cannot be modeled in the one-dimensional one-mass model, and it is anticipated to apply the flow simulation to develop a better artificial vocal fold.

Index Terms: vocal fold, one-mass model, compressible flow simulations, reed.

1. Introduction

The human sound generation process occurs by airflow from one's lungs and results in vocal fold vibrations. Pressure of the airflow makes the vocal folds vibrate only if sufficiently strong pressure is applied and the vocal folds are tensioned properly, and this vibration leads to the generation of audible pressure pulses called laryngeal sound sources.

The sound generation process has been an area of interest for researchers, and many researchers have been trying to describe this phenomenon by computational models. Firstly, lumped-element models like the one-mass model and the two-mass models have been developed [1-2]. These models use an equation of motion to model the phenomenon of vocal folds' movement by considering spring, lumped-mass, and damper systems. The one-mass model proposed by Flanagan and Landgraf [1] treated the vocal fold as a single lumped-mass having a spring and viscous damping. It is the simplest type of model to obtain the vocal fold displacement**.** The two-mass model given by Ishizaka and Flanagan [2] duplicated principal features of relative motion between upper and lower vocal fold by introducing a coupling stiffness between both masses. By the virtue of these models, we could predict vocal folds' displacement, velocity, and glottal area variation**.**

On the other hand, many researchers have been trying to make a replica that can exactly re-iterate the human voice, which can help in magnifying the physiological process of human voice production for better understanding and can be used for medical purposes and as instruments [3]. The earliest of such models was developed by Von Kempelen known as the first speaking machine and discussed by Dudley and Tranoczy [4], indicating that this machine can be used to produce various sounds and can be considered as speech imitating devices. Recently, for educational purposes, the reed-type artificial vocal fold has been developed by Arai [5], in order to demonstrate the fact that reed-type vocal fold geometry can be used as an excellent tool to teach speech sciences to all the students from elementary to university level. Experimentations performed on the artificial vocal folds by Arai. [5] suggested that they can be used to reproduce a human sound.

Studies were also conducted to make reed-type instruments to generate musical sounds. Hikichi and Osaka [6] conducted a study to measure resonance frequencies and reed vibrations of a Japanese reed instrument "sho" to construct physical models of the instruments. Yokoyama et al. [7] and Yoshinaga et al., [8] performed flow simulations based on compressible Navier-Stokes equations on a single-reed instrument. The results showed that the spectral characteristics were predicted by the simulation up to the frequency range of 13th harmonics. While the sound generation mechanism of the reed instrument was investigated in detail, there are very few simulations conducted on the reed-type artificial vocal fold.

The present research aims to evaluate that whether the compressible flow simulation performed on the reed-type artificial vocal fold is effective enough to predict the sound generated by the artificial vocal fold. The flow and sound generations were expressed with compressible Navier-Stokes equations, while the reed motion was calculated with a one-dimensional beam equation. In addition, the artificial vocal fold was simulated with one-mass modeling and compared with the flow simulations. The sound pressure levels for one mass model and compressible flow simulations were calculated and compared with those measured in experimental setups.

http://dx.doi.org/10.21437/Interspeech.2021-929

2. Materials and Methods

2.1. Artificial vocal fold

The geometry of the reed-type artificial vocal fold is shown in Fig. 1. Unlike the original vocal folds, the artificial vocal fold has only one reed enclosed in a retainer. This geometry of reed and retainer tries to replicate to and fro movement of vocal folds, which is essential in producing sound. General-purpose thermoplastic polymer known as Polyethylene terephthalate (PET) was used as a reed material which gives the stable oscillation. Reed has a total length of 32 mm, with an effective vibrating length of 22 mm. A portion of the reed is fixed to the base part of the retainer. The width of the reed is 10 mm and the thickness is 0.2 mm. These dimensions were determined to reproduce fundamental frequency of human vocal folds.

The retainer made up of nylon resin has a total length of 30 mm, with a curved tip with a radius of 30 mm. The outlet part of the reed has a rectangular cross-section with an area of 24 mm^2, a depth of 4 mm, and a width of 6 mm. The curved tip of the retainer is at the inlet side where the air is coming along with the subglottal pressure, and the flow exits the vocal fold geometry from the rectangular cross-section. The reed and retainer are enclosed in an acrylic cylinder having an inner diameter of 30 mm and a length of 55 mm.

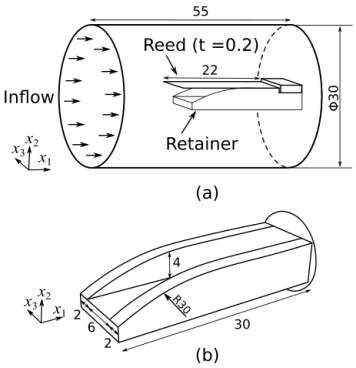

Figure 1: *Schematic diagram of reed-oscillated vocal fold replica: (a) artificial vocal folds geometry enclosed in an acrylic cylinder, (b) retainer geometry.*

2.2. One-mass model for the reed-type vocal fold

Since reed is a single rigid mass and effects of structural viscosity are not considered, the simplest one-mass model with a single degree of freedom for vocal folds [1] was applied to the reed-type artificial vocal fold. By utilizing the model, we predicted the reed displacement, subsequent flow velocity, and changes in the flow rate. In order to simplify the model, it is considered that flow induced reed oscillations are in vertical direction only. The pressure in the retainer P_b is estimated by using Bernoulli's equation

$$P_b = \frac{1}{2}\rho|U_g|^2 A_g^{-2} \quad (1)$$

considering the air density ρ and flow rate of air U_g passing through the retainer. The glottal area A_g is calculated as

$$A_g = A_{go} + ld \quad (2)$$

where A_{go} is the original glottal area, l is the width of the retainer channel (6 mm), and d is the size of the assumed mass (5 mm). Pressures acting at the initial and endpoints of the reed are obtained by

$$P_1 = P_s - 1.37P_b \quad (3)$$

$$P_2 = -0.5P_b \quad (4)$$

using inlet pressure P_s and the pressure obtained by the Bernoulli's equation. The average of these pressures is then used to obtain the flow-induced force acting on the reed surface as

$$F = \frac{1}{2}(\mathrm{P}_1 + \mathrm{P}_2)\, ld. \quad (5)$$

By applying this force to an equation of motion of the reed, the reed displacement is calculated as

$$M\ddot{x} + c\dot{x} + kx = F \quad (6)$$

where M is the mass of the vocal folds, $c = 2\sqrt{kM}$ is the damping constant and k is the coefficient of spring stiffness and was set as 5.6 N/m to match the fundamental frequency. The equivalent Young's modulus is calculated as $Y = kL/S = 0.056$ MPa, where L is the length of the spring and S is the cross-sectional area of the oscillating mass. In contrast to compressible flow simulation, one mass model is considering reed as a rigid lumped mass instead of a continuous one, hence the equivalent Young's Modulus was smaller than that of flow simulation.

Assumptions are made for this model considering the fact that for position less than a critical position of reed (position at which glottal area is zero, $x < -4$ mm), glottal area and flow rate are zero. For all the reed positions which are lower than or equal to the critical position, the effect of a contact force of 5×10^{-6} N/m is taken into account. Viscous damping c is only taken into account while this damping appears. All the other situations are considered as $c = 0$. Also, it is considered that for all the reed positions higher than the initial position ($x > 0$), the varied glottal area is fixed to the maximum cross-sectional area of 24 mm^2, since the flow can exit only through the area of the retainer outlet. In view of all these assumptions, the dynamics of reed motion are obtained by using the equation of motion. The time integration is performed by the Euler method with a time step of 1.0×10^{-6} s.

By using the flow rate, the far-field sound pressure p' was predicted by [9]

$$p' = \frac{1}{4\pi\kappa}\frac{\rho}{r}\frac{dU_g}{dt} \quad (7)$$

where κ is specific heat and r is propagating distance.

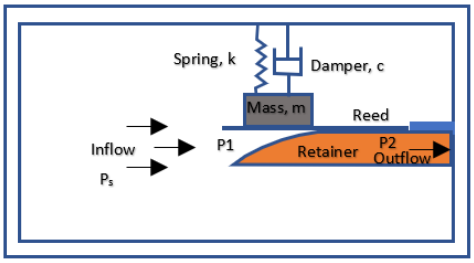

Figure 2. *Schematics of the one mass model.*

2.3. Numerical flow simulation

The vocal fold replica on which the compressible flow simulation is performed is shown in Fig. 3. Three-dimensional

compressible Navier Stokes equations are considered to obtain the reed displacement, flow, and acoustic fields around the oscillating reed. To obtain results of flow and acoustic fields for the complex shape, volume penalization (VP) method, one of the immersed boundary methods proposed by Liu and Vasilyev [10],

$$\boldsymbol{Q}_t + (\boldsymbol{F} - \boldsymbol{F}_v)_{x_1} + (\boldsymbol{G} - \boldsymbol{G}_v)_{x_2} + (\boldsymbol{H} - \boldsymbol{H}_v)_{x_3} = \boldsymbol{V} \quad (8)$$

was used, where $\boldsymbol{Q}$ is the vector of conservative variables. $\boldsymbol{F}$, $\boldsymbol{G}$, and $\boldsymbol{H}$ are inviscid flux vectors, and $\boldsymbol{F}_v$, $\boldsymbol{G}_v$, and $\boldsymbol{H}_v$ are viscous flux vectors. The VP term $\boldsymbol{V}$ was calculated as

$$V = -(1/\phi - 1)\chi \begin{pmatrix} \partial \rho u_i / \partial x_i \\ 0 \\ 0 \\ 0 \\ 0 \end{pmatrix} \quad (9)$$

where ρ is the air density and ϕ is the porosity of the medium. To obtain the almost complete reflectivity (99%) of sound waves on the wall, the value of ϕ was set to 0.25. The mask function χ was given as:

$$\chi = \begin{cases} \min(1, |d/\Delta x_2|) & \text{(inside object)} \\ 0 & \text{(outside object)} \end{cases} \quad (10)$$

where Δx_2 is the grid size in the vertical direction, and d is the distance between a surface of the moving wall and the closest grids. Spatial derivatives were solved by using a sixth-order accuracy compact finite difference scheme [11]. Time integration was done by a third-order Runge Kutta Scheme. Details of flow simulation are presented by Yokoyama et al. [12].

Displacement of the reed with homogenous material is modeled with a one-dimensional beam equation by Avanzini and Van Walstijn [13] to estimate the reed position:

$$\rho_r S \left[\frac{\partial^2 y}{\partial t^2} + \gamma \frac{\partial y}{\partial t}\right] + \frac{\partial^2}{\partial x_1^2}\left[YI\left(1 + \eta \frac{\partial}{\partial t}\right)\frac{\partial^2 y}{\partial x_1^2}\right] = F_{\text{ext}} \quad (11)$$

where ρ_r is the density of the reed, y is the reed displacement, S is the area of the cross section of reed, Y is Young's modulus, I is the second moment of area, γ is the damping coefficient, η is the viscous coefficient of the reed having a value of 1 s^{-1}, and F_{ext} is the external force. External force constitutes the force of fluid on reed and force of contact with the retainer.

The fluid force F_{fluid} was calculated by integrating pressure p on the reed surface, and the contact force $F_{contact}$ was calculated by modeling elastic and dissipative forces on the retainer.

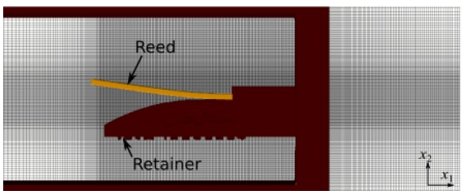

Figure 3. *Computational grids for the reed-type artificial vocal fold.*

2.4. Experimentation

An experimental setup to measure the generated sound is shown in Fig 4. The airflow was supplied to the model by an air compressor (SOL-2039, Misumi, Japan). This airflow was supplied to the artificial vocal fold via a tube having an inner diameter of 16 mm. A flow valve (IR2000-02, SMC, Japan), and a flow meter (PFM750-01, SMC, Japan) were installed on the respective pipeline in between the compressor and inlet side of the geometry, to regulate the airflow with a flow rate of 600 cm^3/s. In order to smooth out the flow of air and to prevent any distractions or sounds coming from any external source other than compressor lines, a silencer with honeycomb and urethane filter was installed in between the cylinder of the artificial vocal fold and the air tube coming from the compressor.

A microphone (type 4939, Bruel & Kjaer, Denmark) was placed at a distance of 100 mm to the outlet end of the retainer to record the generated sound. A sound waveform was recorded for 5 s with a sampling frequency of 50 kHz. The sound was measured in an anechoic chamber with a volume of 8.1 m^3. The parameters for the computation and experiment are summarized in Table 1.

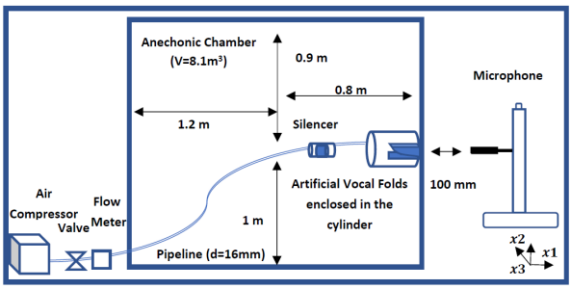

Figure 4: *Experimental setups.*

Table 1: *Parameters for experimentation, simulation and one-mass model*

	Flow simulation	Experiment	One-mass model
Density of the reed ρ_r (kg/m^3)	2000	1400	1400
Young's Modulus Y (MPa)	4200	4200	0.056
Damping Coefficient γ (s)	6.0×10^{-7}	-	0.0137
Time Step Δt (s)	1.0×10^{-7}	-	1.0×10^{-6}
Inlet Pressure P_s (Pa)	800	-	800

3. Results

Sound spectra obtained by the experiment, one-mass model, and flow simulation are plotted in Fig. 5. The fundamental frequencies of the experiment, the one-mass model, and the flow simulation were 135, 131, and 134 Hz, respectively. The amplitude at the fundamental frequency of the experiment was predicted by both model and simulation. In addition, the sound pressure level of the flow simulation almost matched with that of the experimentation up to 2500 Hz, whereas the pressure amplitudes obtained by the one-mass model underestimated those of the experimentation above 300 Hz.

Reed displacement obtained by the one-mass model was compared with that of the compressible flow simulation in Fig. 6. The time on the horizontal axis is normalized by a period of the fundamental frequency. Time t = 0 corresponds to the closed

position of reed. A stable sinusoidal waveform was obtained with an approximate amplitude of 8 mm for the one-mass model, whereas the triangular waveform was obtained with the amplitude of 8 mm for the compressible flow simulation. The curves of the model and the simulation intersected each other in the opening and closing phases. However, the maximum amplitude in both the cases was 8 mm, and the result of the one-mass model was fairly in agreement with the flow simulation.

The simulated time variations of flow rate are plotted in Fig. 7. A square waveform is obtained in one-mass model, while the waveform of flow simulation had round curves in both opening and closing phases. In both curves, the flow rate was almost zero at $t/T = 0$, then, the flow rate increased to the maximum of 600 cm^3/s. The maximum value remained almost constant for $t/T = 0.6$ and it sharply reduced to zero at the closing of the reed.

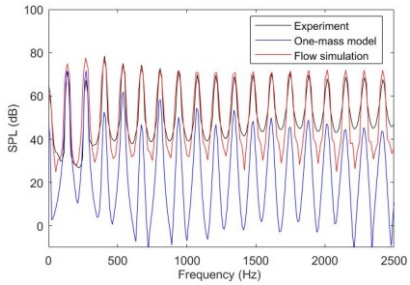

Figure 5 *Sound spectrum of experiment, one-mass model and flow simulation.*

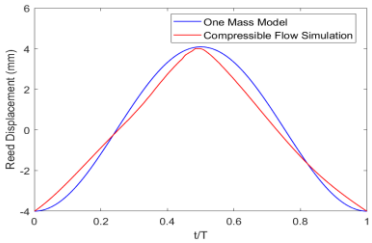

Figure 6: *Reed displacement results by one-mass model and compressible flow simulation.*

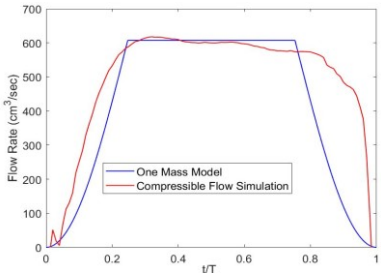

Figure 7: *Flow rate results by one-mass model and compressible flow simulation.*

Flow fields of compressible flow simulation are visualized in Fig. 8 for the opening to the closing phase of reed. Figure 8 (a), (b), and (c) show the flow fields when reed is moving upward in opening phase of cycle. In the closed phase, airflow with higher velocity on the reed surface can be seen in Fig. 8(c). Meanwhile, the closing phase is shown in Fig. 8 (d), (e), and (f). When reed just started to open, the airflow with the minimum velocity was observed in the retainer.

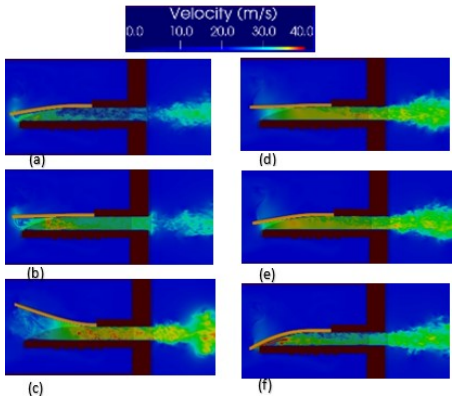

Figure 8: *Velocity magnitudes at the centre of the retainer: (a) t/T = 0.15, (b) t/T = 0.25, (c) t/T = 0.5, (d) t/T = 0.7, (e) t/T = 0.85, (f) t/T = 1.0.*

4. Discussion and Conclusions

As shown in Fig. 5, the sound pressure level obtained by the one-mass model underestimated those of the simulation and experimentation. This was caused by less steep curve of flow rate in the one-mass model compared to the flow simulation. This less steep curve gives the smaller density and pressure fluctuations in artificial vocal fold and ultimately lead towards the smaller amplitude of the sound pressure level as described in Eq. (7) [10].

Overall curve for the reed displacement of the one-mass model agreed with the flow simulation, especially at the maximum value of 600 cm^3/s. However, the curve for the flow simulation showed a rapid increase and decrease, and curve was not as symmetrical as that obtained by one-mass model. These differences were caused by flow retention stored in the retainer and resulted in the difference of the flow field as shown in Fig. 8 (b) and (d). In contrast to the flow simulation, these phenomena were not modeled in the one-mass model which resulted in gradually varying flow rate, hence giving a smooth sinusoidal curve for the displacement and smaller acoustic amplitudes in the higher frequency range.

In this study, the sound generated by reed-type artificial vocal fold was predicted by lumped-mass modeling as well as the compressible flow simulation, and verification was done by the experiment. It was shown that flow simulation efficiently predicted the sound production by artificial vocal fold, while one-mass model underestimated the acoustic amplitudes in higher frequency range. Discrepancies were found in the time variation of flow rate in opening and closing phases, which can be explained by the flow retention which is not modeled in one-mass model. Present work can be further improved by incorporating the effect of structural viscosity and extending it to multi-mass modeling for better understanding of the sound generation phenomenon through the reed-oscillated vocal folds for future works.

5. Acknowledgements

This work was supported by MEXT as Program for Promoting Researches on the Supercomputer “Fugaku” (hp200123, hp200134), JSPS KAKENHI (JP21K02889, JP20K14648), and JSPS Grant-in-Aid for Scientific Research on Innovative Areas (JP20H04999).

6. References

[1] J. Flanagan and L. Landgraf, "Self Oscillating Source for Vocal Tract Synthesizers," *IEEE Transactions on electro and audio acoustics,* vol. 16, no. 1, pp. 57-64, 1968.

[2] K. Ishizaka and J. Flanagan, "Synthesis of voiced sounds from a two-mass model of the vocal cords," *Bell System Technology,* vol. 51, no. 6, pp. 1233-1268, 1972.

[3] R. R. Riesz, "Description and demonstration of an artificial larynx," *The Journal of the Acoustical Society of America,* vol. 1(2A), pp. 273-279, 1930.

[4] H. Dudley and T. Tarnoczy, "The Speaking Machine of Wolfgang von Kempelen," *The Journal of Acoustical Society of America,* vol. 22, no. 2, pp. 151-166, 2005.

[5] T. Arai, "Education in acoustics and speech science using vocal-tract models," *The Journal of the Acoustical Society of America,* vol. 131, pp. 2444-2454, 2007.

[6] T. Hikichi and N. Osaka, "Measurements of the resonance frequencies and the reed vibration of the sho," in *Acoust. Sci. & Tech.*, 2002.

[7] H. Yokoyama, M. Kobayashi and A. Iida, "Analysis of flow and acoustic radiation in reed instruments by compressible flow simulation," *Acoustic Science and Technology,* vol. 41, no. 5, pp. 739-750, 2020.

[8] T. Yoshinaga, H. Yokoyama, T. Shoji, M. Akira and I. Akiyoshi, "Global numerical simulation of fluid-structure-acoustic interaction in a single-reed instrument," *The Journal of Acoustical Society of America,* vol. 149, no. 3, pp. 1623-1632, 2021.

[9] M. J. Lighthill, "On Sound Generated Aerodynamically. I. General Theory," *Proceedings of the Royal Society,* vol. 211, pp. 564-587, 1952.

[10] Q. Liu and O. Vasilyev, "A Brinkman Penalization Method for Compressible flow in complex geometries," *Journal of Computational Physics,* vol. 227, no. 2, pp. 946-966, 2007.

[11] S. K. Lele, "Compact finite difference schemes with spectral-like resolution," *Journal of Computational Physics,* vol. 103, no. 1, pp. 16-42, 1992.

[12] H. Yokoyama, M. Akira, O. Hirofumi and I. Akiyoshi, "Direct Numerical Simulation of fluid-acoustic interactions in a recorder with tone hole," *The Journal of Acoustical Society of America,* vol. 138, no. 2, pp. 858-873, 2015.

[13] F. Avanzini and M. Van Walstijn, "Modeling the mechanical response of the reed mouth piece lip system of clarinet. Part I. Aone dimensional distributed model," *Acta Acoustica united with Acoustica,* vol. 90, no. 3, pp. 537-547, 2004.